Soft Matter

PAPER

View Article Online
View Journal | View Issue

Cite this: *Soft Matter*, 2017, **13**, 1493

Direct demonstration of lipid phosphorylation in the lipid bilayer of the biomimetic bicontinuous cubic phase using the confined enzyme lipid A phosphoethanolamine transferase†

Leonie van 't Hag,[abc] Anandhi Anandan,[d] Shane A. Seabrook,[c] Sally L. Gras,[abe] Calum J. Drummond,[cf] Alice Vrielink*[d] and Charlotte E. Conn*[f]

Received 4th November 2016,
Accepted 18th January 2017

DOI: 10.1039/c6sm02487d

rsc.li/soft-matter-journal

Retention of amphiphilic protein activity within the lipid bilayer membrane of the nanostructured biomimetic bicontinuous cubic phase is crucial for applications utilizing these hybrid protein–lipid self-assembly materials, such as in *meso* membrane protein crystallization and drug delivery. Previous work, mainly on soluble and membrane-associated enzymes, has shown that enzyme activity may be modified when immobilized, including membrane bound enzymes. The effect on activity may be even greater for amphiphilic enzymes with a large hydrophilic domain, such as the *Neisserial* enzyme lipid A phosphoethanolamine transferase (EptA). Encapsulation within the biomimetic but non-endogenous lipid bilayer membrane environment may modify the enzyme conformation, while confinement of the large hydrophilic domain with the nanoscale water channels of a continuous lipid bilayer structure may prevent full function of this enzyme. Herein we show that *Nm*EptA remains active despite encapsulation within a nanostructured bicontinuous cubic phase. Full transfer of the phosphoethanolamine (PEA) group from a 1,2-dioleoyl-*glycero*-phosphoethanolamine (DOPE) doped lipid to monoolein (MO), which makes up the bicontinuous cubic phase, is shown. The reaction was found to be non-specific to the alkyl chain identity. The observed rate of enzyme activity is similar to other membrane bound enzymes, with complete transfer of the PEA group occurring *in vitro*, under the conditions studied, over a 24 hour timescale.

Introduction

Lipidic self-assembly materials, consisting of surfactant bilayer structures that mimic the cell membrane environment, can be used to encapsulate amphiphilic proteins and peptides.[1] The inverse bicontinuous cubic phases (Q_{II}) are particularly suited for this purpose, due to their continuous three-dimensional bilayer structure and amphiphilic nature, which can incorporate both the hydrophobic and hydrophilic domains of proteins.[2,3] For this reason, the cubic phase nanostructure may assist in the retention of protein activity following the encapsulation of soluble, peripheral and integral membrane proteins.[1] Additionally, the high surface area to volume ratio of these structures allows incorporation of relatively large amounts of protein or peptide. The resulting self-assembling hybrid protein–lipid materials are increasingly used in applications such as in *meso* crystallization of membrane proteins,[4] as drug delivery vehicles for amphiphilic and hydrophobic therapeutics and imaging agents,[5–9] as biosensors[10] and biofuel cells.[11]

The relationship between the lipid nanomaterial and the encapsulated protein must be understood in order to fully develop and apply hybrid protein–lipid self-assembly materials. Retention of the bilayer membrane based cubic nanostructure is essential to the use of these materials in select applications, such as in *meso* crystallization and drug delivery. A number of recent studies have therefore investigated changes to the lipidic nanostructure caused by the incorporation of amphiphilic proteins and peptides within the bicontinuous cubic phases.[1,12–17] Hydrophobic mismatch, hydrophilic domain size and charge were found to be the most important factors affecting the nanostructure.

[a] *Department of Chemical and Biomolecular Engineering, The University of Melbourne, Parkville, Victoria 3010, Australia*
[b] *Bio21 Molecular Science and Biotechnology Institute, The University of Melbourne, Parkville, Victoria 3010, Australia*
[c] *CSIRO Manufacturing, Clayton, Victoria 3168, Australia*
[d] *School of Chemistry and Biochemistry, University of Western Australia, Crawley, Western Australia 6009, Australia. E-mail: alice.vrielink@uwa.edu.au*
[e] *The ARC Dairy Innovation Hub, The University of Melbourne, Parkville, Victoria 3010, Australia*
[f] *School of Science, College of Science, Engineering and Health, RMIT University, Melbourne, Victoria 3001, Australia. E-mail: charlotte.conn@rmit.edu.au*

† Electronic supplementary information (ESI) available: (1) ESI-TOF MS data of RP-HPLC fractions as shown in Fig. 3(A and D). (2) Figures showing reproducibility of the SAXS results as shown in Fig. 5–7. (3) High-throughput data with DMPE, presented in individual graphs for every % w/w DMPE. See DOI: 10.1039/c6sm02487d

In addition, retention of the activity of the protein within the lipidic material is essential if the protein is to be used in its functionally active form.

While spectroscopic techniques that investigate the conformation of the proteins have been used as an indirect measure for protein activity,[13,15,18,19] direct measurements of the activity of amphiphilic proteins within the bicontinuous cubic phase remain challenging. The enzyme activity of soluble oxidases in the nanoscale water channels of the cubic phase has been reported, for example for glucose oxidase,[10,20,21] ceruloplasmin,[20] lactate oxidase,[21] urease,[21] creatinine deiminase,[21] cholesterol oxidase,[10] horseradish peroxidase[22,23] and laccase.[11,24] Increased stability and activity was found for the mostly hydrophilic membrane bound enzyme fructose dehydrogenase when immobilized within the cubic phase compared to when present in buffer solution.[25] Ion transport across the lipid membrane by the purely hydrophobic proteins and peptides OmpF,[16] EcClC,[26] and a synthetic four-helix bundle[27] has also been reported. Ligand binding assays were recently used to show that the dopamine D2L receptor retained a conformation that preserves the ligand binding region when encapsulated in some bicontinuous cubic phases.[28] However, to our knowledge the activity of a large amphiphilic protein, which has amphiphilic donor and receiver substrates, when encapsulated in the bicontinuous cubic phase has not yet been reported. These systems differ in that the hydrophilic domain must be confined within the nanoscale aqueous channel network of the cubic phase. Retention of protein activity is particularly important for these proteins, such as the large, non-rigid, hydrophilic domains from G-Protein Coupled Receptors (GPCRs) that are commonly removed or modified for successful crystal growth using in *meso* crystallization.[29] These proteins are also of critical importance, as 60% of all pharmaceutical compounds currently on the market target GPCRs.[30] The size of the hydrophilic domain is therefore also of great interest for applications of the bicontinuous cubic phase.

In this study the activity of the amphiphilic enzyme lipid A phosphoethanolamine transferase from *Neisseria meningitidis* (*Nm*EptA) within the nanostructured bicontinuous cubic phase of monoolein (MO) is investigated. MO is the most commonly used bicontinuous cubic phase forming lipid[31] and is readily available at low cost. It forms a robust diamond cubic Q_{II}^{D} phase at room temperature and in excess water, Fig. 1(A), with a lattice parameter of ~104 Å. The typical lipid bilayer thickness within the MO cubic phase is ~32 Å, with water channels of ~51 Å in diameter.[32,33] Branched chain lipids such as phytantriol have a significantly higher lateral bilayer pressure profile, which in a recent study was found to be unfavorable for the encapsulation of transmembrane peptides and proteins.[34,35]

Lipid A phosphoethanolamine transferase (EptA) (62.2 kDa) from the Gram-negative bacteria *Neisseria meningitides* and *N. gonorrhoeae* is a cytoplasmic membrane localized enzyme consisting of five transmembrane α-helices and a large hydrophilic domain ~45 × 45 × 68 Å in size, Fig. 1(B). EptA modifies the lipid A headgroups of lipopolysaccharides (bacterial endotoxin molecules), with phosphoethanolamine (PEA).[37] This modification of the bacterial endotoxin prevents the binding of negatively charged antibiotics, such as polymyxin and naturally occurring cationic antimicrobial peptides (CAMPs), such as defensins, to the cell membrane. Additionally, this modification confers resistance to both the innate immune clearance mechanisms during bacterial colonization and the treatment of invasive infections with polymyxin.[38] An improved understanding of the activity and catalytic mechanism of EptA can lead to the development of novel treatments for Gram-negative bacterial infections such as gonorrhea. A crystal structure of the soluble domain of *Nm*EptA showed components of the enzyme active site, Fig. 1(B), but suggested that the full substrate binding site would require the transmembrane domain,[36] thus emphasizing the need to characterize the full length amphiphilic protein. A crystal structure of the full length *Nm*EptA protein has since been obtained from detergent micelles by Anandan *et al.* (*PNAS*, in press). This structure shows the enzyme in a compact conformation with a single molecule of *n*-dodecyl β-D-maltoside (DDM) bound to the proposed substrate binding site, leading to the hypothesis that this structure mimics the phosphatidylethanolamine substrate

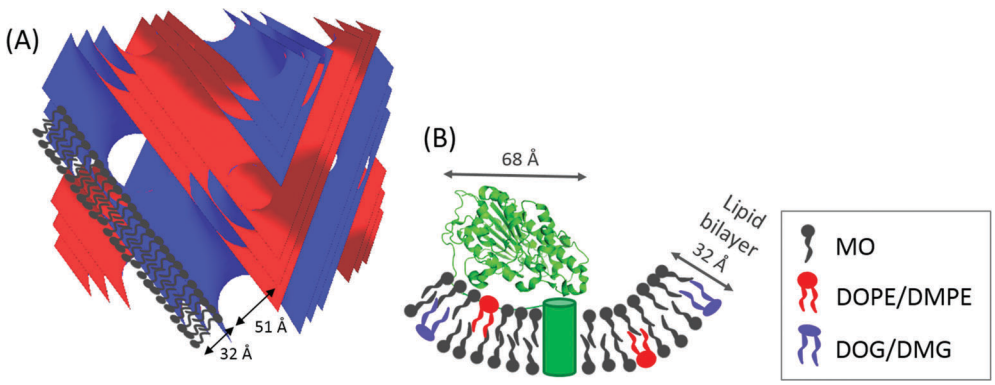

Fig. 1 (A) Schematic representation of self-assembled diamond cubic Q_{II}^{D} phase, with typical dimensions for lipid bilayer thickness and water channel diameter indicated for monoolein (MO). The blue and red surfaces indicate the Q_{II}^{D} phase structure adopted by the amphiphile. (B) Lipid A PEA transferase protein structure (PDB ID: 4KAV and information about the location of the transmembrane domain from A. Anandan, G. L. Evans, K. Condic-Jurkic, M. L. O'Mara, C. M. John, N. J. Phillips, G. A. Jarvis, S. S. Wills, K. A. Stubs, I. Moraes, I. Moraes, C. M. Kahler and A. Vrielink, *PNAS*, 2017, in press) and the corresponding dimensions determined from the crystal structure.[36] The transmembrane α-helices are indicated by the green cylinder in a lipid bilayer formed by MO doped with DOPE/DMPE, and with the formation of DOG/DMG.

bound conformation. Molecular dynamics simulations and intrinsic fluorescence studies also indicate that the protein undergoes conformational changes, possibly to accommodate the binding of the two different types of lipid substrates: the small donor substrate, phosphatidylethanolamine, and the larger receiver substrate, lipid A containing lipooligosaccharide. This conformational flexibility may alter the total length of the enzyme from that observed in the crystal structure.

In vivo *Nm*EptA transfers the PEA group from PEA containing lipids such as 1,2-dimystroyl-*glycero*-phosphoethanolamine (DMPE) in the inner- and outer membrane of the bacteria and attaches this molecule to lipid A as described above. In this study, the activity of *Nm*EptA in the nanostructured cubic phase of MO was studied in the presence of the substrate DMPE, or 1,2-dioleoyl-*glycero*-phosphoethanolamine (DOPE). DMPE and DOPE were compared to investigate the specificity of the enzyme to phospholipids with saturated alkyl chains (DMPE), as commonly found in Gram-negative bacteria, or with unsaturated alkyl chains (DOPE), which are more miscible with the unsaturated alkyl chains of MO.[39] The chemical structures and molecular weights of the lipids used are shown in Table 1. In the first part of the paper, the conversion of DMPE to 1,2-dimyristoyl-glycerol (DMG) and of DOPE to 1,2-dioleoyl-glycerol (DOG) by *Nm*EptA in the bulk cubic phase of MO was investigated using reversed phase – high performance liquid chromatography (RP-HPLC) and electrospray ionization – time-of-flight (ESI-TOF) mass spectroscopy (MS). We also used high-throughput techniques, including high-throughput sample preparation and high-throughput synchrotron small-angle X-ray scattering (SAXS), to investigate the additional effect of *Nm*EptA protein concentration and the concentration of either DMPE or DOPE.

Experimental section

Materials

MO, Hepes, NaCl, *n*-dodecyl β-D-maltoside (DDM) were purchased from Sigma-Aldrich (St Louis, MO, USA). DOPE, DMPE, DOG and DMG were obtained from Avanti polar lipids (Alabaster, AL, USA). Ethanol and chloroform were bought from Merck & Co, Inc. (Whitehouse Station, NJ, USA). Methanol was purchased from Fischer Scientific Pty Ltd (Scoresby, VIC, Australia). SD-2 96-well crystallization plates were purchased from IDEX Corp (Rohnert Park, CA, USA).

*Nm*EptA expression and purification

Recombinant *Nm*EptA was expressed and purified according to the procedures detailed in Anandan *et al.* (*PNAS*, in press). Briefly, recombinant C terminal His_6-tagged *Nm*EptA was expressed in *E. coli* strain (BL21(DE3) pLysS). Cells were harvested by centrifugation (12 290 × *g* for 1 hour at 4 °C) and lysed in 50 mM Na phosphate pH 7.5 containing 300 mM NaCl and 1 mM PMSF using an Emulsiflex C5 high-pressure homogenizer (Avestin, Mannheim, Germany). The membranes were isolated by ultracentrifugation of the lysate at 185 511 × *g* for an hour at 4 °C. *Nm*EptA was solubilized from the membranes by incubating the isolated membranes with 1% w/v DDM in 50 mM Na phosphate pH 7.5 containing 300 mM NaCl and 1 mM PMSF for 4 hours. The solubilized *Nm*EptA was separated from the membrane debris by ultracentrifugation at 185 511 × *g* for an hour at 4 °C.

Solubilized *Nm*EptA was purified by metal chelating chromatography and size exclusion chromatography. The supernatant from ultracentrifugation was applied to a HisTrap crude extract chelating affinity column (GE Healthcare, Buckinghamshire, UK) equilibrated with binding buffer (50 mM sodium phosphate pH 7.5, 300 mM sodium chloride, 20 mM imidazole and 0.023% w/v DDM (3 × CMC)) using an ÅKTApurifier FPLC system (GE Healthcare). Bound *Nm*EptA was eluted using the elution buffer (50 mM sodium phosphate pH 7.5, 300 mM sodium chloride, 500 mM imidazole, 0.023% w/v DDM). The eluted protein was buffer exchanged into 50 mM sodium phosphate pH 7.5, 150 mM sodium chloride and 0.023% w/v DDM using a PD-10 desalting column (GE Healthcare) and applied to a size exclusion chromatography column (Superdex 200 10/30, GE Healthcare)

Table 1 Chemical structure and molecular weight (M_w) for the lipids used in this study. An additional mass observed by ESI-TOF analysis (M_w + 18) with an ammonium adduct is also shown. The lattice parameters (lp) in excess hydration and at room temperature (SAXS result) are also presented. Q_{II}^D is the diamond cubic phase, L_α is the lamellar phase, H_{II} the inverse hexagonal phase and Fl is a fluid isotropic phase

Lipid	Chemical structure	M_w (g mol^{-1})	M_w + 18 (g mol^{-1})	Phase + lp(A)
Monoolein (MO)	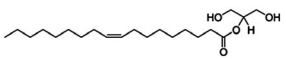	356.5	374.5	Q_{II}^D 104
Monoolein phosphoethanolamine (MOPE)	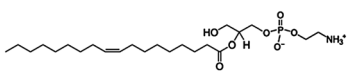	479.7		
Dioleoyl-glycerol (DOG)	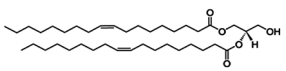	621.0	639.0	Fl
Dioleoyl-phosphoethanolamine (DOPE)	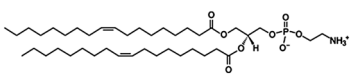	744.0		H_{II} 74
Dipalmitoyl-glycerol (DMG)	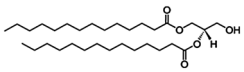	512.8	530.8	L_α 42
Dipalmitoyl-phosphoethanolamine (DMPE)	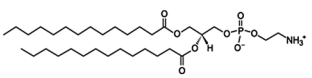	635.9		L_α 51

equilibrated with 50 mM Hepes pH 7.0, 100 mM NaCl and 0.023% w/v DDM. Fractions containing *Nm*EptA eluted from the size exclusion chromatography column were pooled and concentrated using a 100 kDa molecular weight cutoff centrifugal filter unit (Vivaspin 20 MWCO 100 000, GE Healthcare) to 18 mg mL^{-1}, as determined by the absorbance at 280 nm using a calculated molar extinction coefficient for *Nm*EptA (73 980 M^{-1} cm^{-1}).

Sample preparation for *Nm*EptA assay

MO with 10% w/w DOPE was first co-dissolved in ethanol, and MO with 10% w/w DMPE in methanol/chloroform/water (65 : 35 : 8 v/v). The use of different solvents for sample preparation with DOPE and DMPE was necessary due to the limited solubility of DMPE in ethanol. A significant amount of chloroform had to be used to solubilize DMPE but chloroform is not compatible with subsequent sample treatment and analysis procedures. Most of the respective solvent was evaporated under a stream of N_2 and the lipid mixture was then freeze dried. The cubic phase was prepared in coupled Hamilton syringes (Hamilton, Reno, NV, USA) at 40% w/w hydration,[18] starting with the lipid mixture in one syringe and *Nm*EptA at 18 mg mL^{-1} in buffer/DDM or just buffer/DDM solution in the second syringe. A volume of 25 μL of cubic phase was then transferred into a microfuge tube and centrifuged for 2 minutes at 14 500 rpm (Eppendorf, Ontario, Canada) to obtain a smooth surface. An additional 25–50 μL of buffer solution was added to ensure the samples remained hydrated. After the appropriate reaction time, the excess water was removed and the MO/DOPE/*Nm*EptA samples were dissolved in 500 μL of 70% v/v ethanol and the MO/DMPE/*Nm*EptA samples were dissolved in 100 μL methanol/chloroform/ water (65 : 35 : 8 v/v). The MO/DMPE/*Nm*EptA samples were then diluted 500 times in 70% v/v ethanol to reduce the amount of chloroform in the sample. The *Nm*EptA protein was removed from the samples using a Vivaspin 500 centrifuge tube with 10 000 MWCO from Satorius AG (Goettingen, Germany). The resulting lipid solutions at 30 mg mL^{-1} for MO/DOPE and 0.3 mg mL^{-1} for MO/DMPE in 70% v/v ethanol were used for composition analysis.

Lipid composition analysis *Nm*EptA assay

The lipid composition in the *Nm*EptA assay samples was determined after 1, 12 and 24 hours for separate samples using mass spectroscopy (MS) and reversed-phase – high performance liquid chromatography (RP-HPLC). MS was performed using an Agilent 6200 Series ESI-TOF spectrometer from Agilent Technologies (Santa Clara, CA, USA). RP-HPLC was carried out using an Agilent 1200 series HPLC system equipped with a quaternary pump (G1311A) and diode array (DAD)/multiple wavelength detector (G1365B). Lipid separation was performed using a reversed phase ProteCol C18 HQ203 column (SGE, Ringwood, VIC, Australia) with 200 Å pore size, 100 mm × 2.1 mm. The linear gradient was 70–100% methanol (30–0% water) in 30 minutes and 100% methanol from 30 to 45 minutes, with a flow rate of 0.25 mL min^{-1}. Data of a 2,2,2-trifluoroethanol sample was subtracted from the spectra to correct for the baseline. Fractions for ESI-TOF analysis were collected every one minute, in a Corning 96-well plate (Corning, NY, USA).

Plate setup for high-throughput *Nm*EptA assay

Samples for the high-throughput *Nm*EptA assay using small-angle X-ray scattering (SAXS) analysis were prepared in 96-well SD-2 crystallization plates.[40] MO, DOPE and DOG stock solutions were prepared in ethanol at concentrations of 400 mg mL^{-1}, 50 mg mL^{-1} and 50 mg mL^{-1} respectively. A DMG solution was prepared at 50 mg mL^{-1} in ethanol/methanol/chloroform (70 : 15 : 15 v/v). DMPE was dissolved at 25 mg mL^{-1} in methanol/chloroform (50 : 50 v/v) for plates without *Nm*EptA and at 50 mg mL^{-1} in ethanol for plates with *Nm*EptA. A volume of (diluted) lipid solutions was dispensed with the Mosquito robot (TTP Labtech, Cambridge, MA, USA) into the top and bottom subwells of the plates to obtain the required amount of each lipid. In every well 0.21 mg MO with up to 0.03 mg additional DOPE, DOG, DMPE, or DMG was deposited. The largest volume of lipid stock solution was always dispensed last. DMPE was poorly soluble and dispensed as an emulsion. Plates were dried under vacuum for 5–7 days to remove solvent. A volume of 20 μL of water or buffer (50 mM Hepes (pH 7.0), 100 mM NaCl) was dispensed into the reservoirs using the Phoenix robot (Arts Robins Instruments, Sunnyvale, CA, USA). A volume of 0.56 μL of water, buffer, buffer/DDM or *Nm*EptA solution was dispensed on top of the dried lipid films using the Mosquito robot, resulting in 70–73% w/w (excess) hydration in the wells. Samples with *Nm*EptA were measured after 2, 12 and 20 hours equilibration and SAXS patterns were taken at different positions in the well for each time point (top left, top right and bottom within the 1.5 mm diameter well, respectively) to minimize the effect of radiation damage.

Small-angle X-ray scattering (SAXS) measurements

Structural analysis of the cubic phase samples in SD-2 crystallization plates and sandwich plates with Kapton tape was performed at the SAXS/WAXS beamline at the Australian Synchrotron.[41] Data acquisition was performed at 25 °C using a custom-designed, temperature-controlled plate holder. An X-ray wavelength of 1.0332 Å (12.0 keV) was used with a typical flux of 10^{13} photons s^{-1}, 0.2 s exposure time and beam dimensions of ~200 μm × 300 μm. Recording SAXS patterns for all wells in one SD-2 crystallization plate (128 wells) took ~20 minutes, which is significantly faster than the time scales of the enzymatic reaction, which was observed to occur over a time frame of 12–24 hours but not before two hours. A Pilatus 1 M detector was used to record two-dimensional diffraction images. 1-D scattering profiles were obtained by azimuthally averaging the 2-D SAXS images. In the 1-D scattering profiles many orders of diffraction were observed, which allowed unambiguous identification of the bicontinuous cubic, inverse hexagonal and lamellar phases. The IDL-based AXCESS software package and the high-throughput analysis program RapidPhaseIdent were used for data analysis.[42,43]

Results and discussion

*Nm*EptA assay in the bulk bicontinuous cubic phase of MO with DOPE and DMPE

The bulk bicontinuous cubic phase was formed by the lipid MO with the second lipid (DOPE or DMPE) doped within the lipid

bilayer at a concentration of 10% w/w. The amphiphilic *Nm*EptA protein was then incorporated within the nanostructured cubic phase, with the transmembrane α-helices embedded in the lipid bilayer and the hydrophilic domain confined within the nanoscale water channels, as shown in Fig. 1. The substrate binding site of the enzyme is expected to be at the interface between the hydrophobic and hydrophilic domains, which allows the PEA moiety to be captured from lipids such as DOPE and DMPE found within the lipid bilayer. We first studied the transfer of the PEA moiety from DOPE and DMPE by *Nm*EptA in the bulk bicontinuous cubic phase of MO using lipid composition analysis by MS and RP-HPLC. RP-HPLC was used to quantify the lipids present, with identification of the lipid fractions confirmed by MS. Mixtures of pure MO, DOPE, and DOG (49 : 25 : 26 w/w) and MO, DMPE, and DMG (47 : 27 : 26 w/w) in 70% v/v ethanol (in the absence of *Nm*EptA) were initially analyzed to develop these MS and RP-HPLC methodologies.

Three lipid species can be clearly distinguished in the ESI-TOF spectra shown for the pure lipid mixtures in Fig. 2(A) and 4(A). Peaks for DOPE at $m/z = 744$ and DMPE at $m/z = 636$ dominate the spectra, because of the presence of a zwitterion in the PEA moiety: such charged species are analyzed more readily than non-charged species in ESI-TOF mass spectroscopy. The m/z values observed correlate well with the molecular weight of these lipids, Table 1. In contrast, peaks for the uncharged DOG and DMG at $m/z = 639$ and $m/z = 531$ were of much lower intensity, even though they were present at similar concentration in the samples. The m/z values observed were ~18 mass units higher than the molecular weight of the lipids, Table 1. We suggest that these are the analyte adducts of DOG and DMG with ammonium (NH_4^+), as is commonly observed in positive ion ESI,†[44] as applied here. For MO, peaks with $m/z = 357$ and $m/z = 374$ were observed for both lipid mixtures. This again correlates to the molecular weight of MO, as well as its ammonium adduct, Table 1. These data with the pure lipid mixtures confirm that ESI-TOF MS analysis can be used to identify the lipids present in these types of samples.

Note that RP-HPLC analysis was only performed for MO, DOPE, DOG samples and not for MO, DMPE, DMG samples due to the limited solubility of DMPE in ethanol and methanol. The large amount of chloroform needed for solubilization of DMPE prevented loading of sufficient lipid in 70% v/v ethanol or methanol in water onto the column for accurate separation and detection. The MO, DOPE, and DOG lipids were detected with the diode array detector (DAD) signal at 203 nm, similar to previous reports that phospholipids are detected readily at ~206 nm.[45] RP-HPLC fractions were collected every minute for lipid identification by ESI-TOF mass spectroscopy.

MO was found to elute after ~22 minutes, which corresponds to ~92% methanol, Fig. 3(A). The MO peak was found to have a small shoulder at ~21 minutes, which is probably due to the presence of the isomeric 2-monoolein in the sample with >90% 1-monoolein. DOPE and DOG eluted after ~36 and ~38 minutes, respectively, which corresponds to 100% methanol, reflecting the different affinity of these two compounds with the reversed-phase C18-column. The ESI-TOF MS data for the relevant fractions is shown in ESI,† Fig. S1.1. The sequence of elution of MO, DOPE,

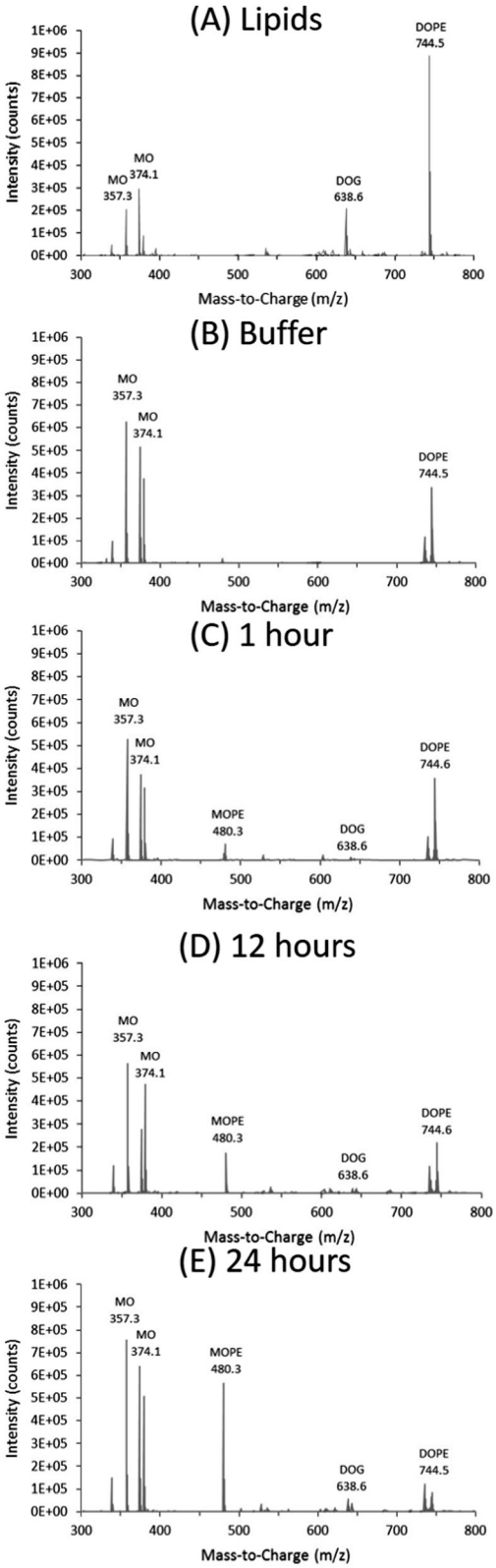

Fig. 2 Masses detected in the *Nm*EptA assay with DOPE by ESI-TOF MS: (A) MO, DOPE, DOG, (B) MO, DOPE, buffer/DDM after 24 hours and MO, DOPE and *Nm*EptA samples after (C) 1 hour, (D) 12 hours and (E) 24 hours.

and DOG is as expected, due to the increased hydrophobicity of these molecules. The relative areas of the peaks for MO, DOPE and DOG (65 : 14 : 21) were found to represent the relative amounts of the different lipids in the sample (65 : 15 : 20 mol mol^{-1}) well, confirming this method can be used for quantification of the relative amount of each of the components present.

In the presence of 18 mg mL^{-1} *Nm*EptA ~10% of the DOPE present was dephosphorylated to DOG after 1 hour (peak areas MO : DOPE : DOG 92 : 7 : 1), as shown by the MS and RP-HPLC data in Fig. 2 and 3 (B–E and B–D respectively) confirming that *Nm*EptA is bioactive in the nanostructured cubic phase. After a further period of 12 hours approximately half of the DOPE molecules were converted to DOG (peak areas MO : DOPE : DOG 92 : 5 : 3) and after 24 hours ~90% of the DOPE was converted to DOG (peak areas MO : DOPE : DOG 95 : 0.5 : 4.5) illustrative of the time dependence of conversion. The data also confirm that the dephosphorylation activity of this enzyme is not specific to saturated phospholipids that are native in the cell membrane of Gram-negative bacteria and the enzyme is also able to dephosphorylate DOPE.

MS analysis of the excess buffer of the bulk cubic phase samples did not detect the PEA moiety removed from the DOPE lipids during the enzymatic reaction and we propose that the PEA moiety (mass ~123 g mol^{-1}) is attached to an OH group of MO. We have termed this lipid MOPE, and it has a mass of ~480 g mol^{-1} (Table 1). The RP-HPLC data contains a peak at a retention time of ~18–19 minutes (~78% methanol), that increases in intensity with reaction time (Fig. 3). The peak corresponds to m/z = 480 and the appearance of this peak can also be seen in the ESI-TOF MS data of the samples after 1, 12 and 24 hours (Fig. 2). Additional ESI-TOF MS data for the relevant fractions of the RP-HPLC result from the sample with MO, DOPE, and *Nm*EptA after 24 hours is shown in ESI,† Fig. S1.2. In the absence of lipid A, we propose that the PEA moiety was attached to MO, confirming the lack of specificity of accepting lipids for this reaction and illustrating that the acceptor is not restricted to lipids that are present in the cell membrane of the Gram-negative bacteria.

For *Nm*EptA samples incubated with DMPE, a small amount of MOPE was formed after 1 hour, as shown by the ESI-TOF MS data in Fig. 4(B–E) indicating that the production of MOPE reaction product was independent of the alkyl chain identity of the substrate, consistent with our suggestion that the PEA moiety has been attached to MO. In this case, the relative intensity of MOPE increased at 12 hours and 24 hours, while the relative intensity of DMPE decreased. The dephosphorylated DMG was observed after 12 hours but not after 24 hours, possibly due to the low sensitivity of the ESI-TOF MS analysis with uncharged compounds.

In summary, the *Nm*EptA assay showed that the enzyme was active in the bulk cubic phase of MO, even though the enzyme is expected to be confined due to the geometrical mismatch of the hydrophilic domain of *Nm*EptA (~45 × 68 Å) in the water channels of the cubic phase (D_w = 51 Å), Fig. 1. After 24 hours the PEA moiety was predominantly attached to MO rather than DOPE or DMPE. The reverse dephosphorylation reaction of MOPE by *Nm*EptA might also occur but this cannot be concluded from this experiment. The rate of transfer of the PEA group by *Nm*EptA is of the same order of magnitude as enzymatic reaction rates of other membrane bound enzymes,[25,46] with full transformation occurring over a 24 hour time period: the overall conversion reaction rate is ~1 μM s^{-1}. This is surprising considering the suggested limited flexibility of the *Nm*EptA enzyme to form different conformations within the nanoscale cubic phase water

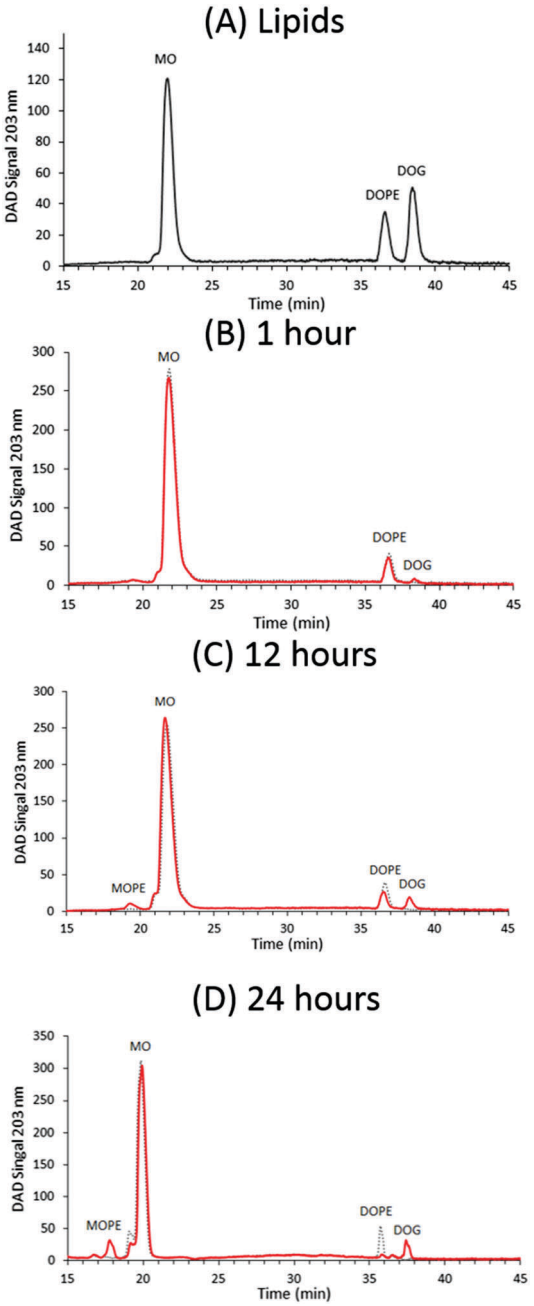

Fig. 3 RP-HPLC data with diode array detector (DAD) signal at 203 nm of *Nm*EptA assay with DOPE. (A) MO, DOPE, DOG. (B–D) MO, DOPE, *Nm*EptA (red solid lines) and buffer/DDM (dashed grey lines) after (B) 1 hour, (C) 12 hours, (D) 24 hours. (A–C) Were measured on the same HPLC system and (D) was analyzed on a different HPLC instrument. The slight differences in peak position and shape between (A–C) compared to (D) are ascribed to difference in HPLC systems.

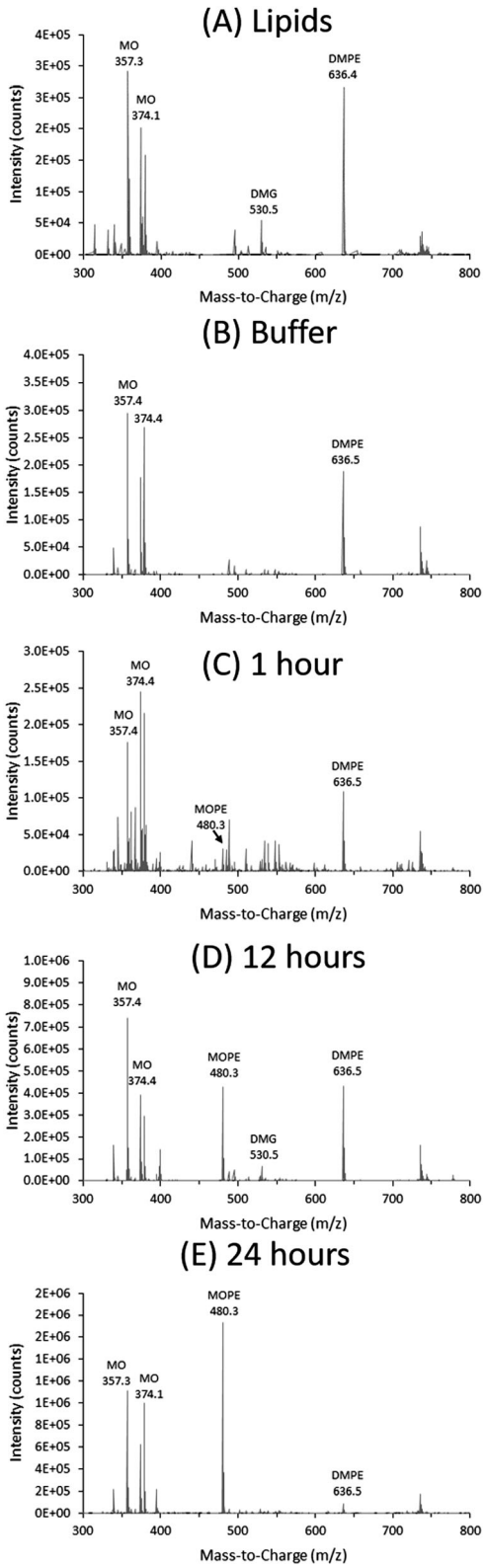

Fig. 4 Masses detected in the *Nm*EptA assay with DMPE by ESI-TOF: (A) MO, DMPE, DMG, (B) MO, DMPE, buffer/DDM after 24 hours, and MO, DMPE and *Nm*EptA samples after (C) 1 hour, (D) 12 hours, (E) 24 hours.

channels. Within the cubic phase disordered nanopockets to accommodate the *Nm*EptA enzyme might have formed.[47,48] The diffusion rate of lipids within the lipid bilayer (the substrate) is typically an order of magnitude slower than soluble components in the water channels,[49] which is also expected to affect the reaction rate. It was found that the enzyme was not specific to native saturated phospholipids, as the PEA moiety of the singly unsaturated lipid DOPE could be transferred to MO with an efficiency similar to the saturated DMPE lipid. Additionally, in the absence of lipid A the PEA moiety was transferred onto the cubic phase forming lipid MO to form MOPE.

High-throughput *Nm*EptA assay: effect of enzyme and substrate concentration

To investigate the effect of *Nm*EptA and substrate (PEA) concentration, a high-throughput assay was performed with ~100 times smaller samples (~0.3 mg) than for the MS and RP-HPLC analysis. High-throughput analysis of enzyme activity is also of prospective use as a screening tool for inhibitors, which could lead to novel treatments of diseases such as gonorrhea and could be applied more readily as an experimental setup for enzyme screening in the cubic phase. Samples were prepared using robotics and the analysis was performed by investigating changes in the nanostructure of the cubic phase using SAXS at room temperature and in excess (~70% w/w) hydration. Samples were prepared in duplicate in the top and bottom subwells of 96-well plates. Reproducibility between the subwells was confirmed, as shown in Supplementary Information 2 (ESI†), with data found to be reproducible (lattice parameters less than 5 Å different) in ~87% of wells. Irreproducible wells, which were more likely for samples with high *Nm*EptA concentration presumably due to the significant impact of the enzyme on the cubic phase nanostructure, were not considered further.

Under these conditions, the lattice parameter of the MO diamond cubic Q_{II}^{D} phase with water was found to be 105.7 Å, in agreement with the literature.[32,33] *Nm*EptA was purified in 50 mM Hepes (pH 7.0) and 100 mM NaCl with 0.023% w/v DDM to solubilize the hydrophobic transmembrane domain. For this reason, the lattice parameter of the diamond cubic Q_{II}^{D} phase of MO was also investigated with excess buffer, and buffer with DDM as a background for comparison. The lattice parameter with 50 mM Hepes (pH 7.0) and 100 mM NaCl was 104.0 Å, and with buffer containing 0.023% w/v DDM at 104.4 Å. This reduction in lattice parameter compared to the value with water can be explained by the presence of 100 mM of NaCl, since NaCl is a kosmotropic salt. Kosmotropic salts can cause a reduction of the water activity,[43,50] resulting in a slightly less hydrated cubic phase. High concentrations of the detergent DDM are known to cause an increase in lattice parameters of the MO cubic phase,[51] but this was not observed here. The Hepes and NaCl components of the buffer were found to dominate the effect of the buffered detergent solution, probably due to the low concentration of DDM in the sample (0.023% w/v). Together these data show the changes in the lipid system due to the buffer components are small and enable subsequent application of the high-throughput system.

Effect of *Nm*EptA on the MO cubic phase. Encapsulation of *Nm*EptA at 0–6 mg mL^{-1} in the diamond Q_{II}^{D} cubic phase of MO

caused a concentration dependent increase in lattice parameter from ~105 Å to ~120 Å, as shown in Fig. 5(A). If the *Nm*EptA protein molecules were only present in the membrane region exposed to bulk water such a linear increase in lattice parameters would not have been observed. Diffusion of the enzyme throughout the cubic phase was also confirmed using fluorescence recovery after photobleaching experiments (unpublished data). *Nm*EptA protein molecules present inside the cubic phase and at the membrane exposed region to bulk water are expected to contribute to the enzyme activity, however, due to its large hydrophilic domain. Data from 9 to 18 mg mL^{-1} *Nm*EptA were found to be more irreproducible and are not presented here. No plateau was observed at the highest concentration studied and no other mesophases were observed. Swelling of the bicontinuous cubic phase upon *Nm*EptA incorporation probably occurred due to the large hydrophilic domain of the enzyme, Fig. 1(B). This was also observed in previous work for other large amphiphilic proteins with either α-helical or β-barrel transmembrane domains: the D2L receptor, Ag43, GPR41 and GPR43, and BamA.[1,12,14,15,52]

Activity of *Nm*EptA in DOPE doped MO. The individual effect of DOPE and DOG on the MO diamond cubic Q_{II}^{D} phase nanostructure was probed to better understand the conversion of DOPE to DOG by *Nm*EptA. The effect of incorporating DOPE and DOG from 0 to 12% w/w is shown in Fig. 5(B). DOPE caused a concentration dependent linear reduction in Q_{II}^{D} lattice parameters from ~105 Å to ~97 Å at 12% w/w, as was also reported in the literature.[39,53] DOG caused a more significant concentration dependent linear reduction in Q_{II}^{D} lattice parameters, down to ~86 Å at 8% w/w, with formation of the inverse hexagonal H_{II} phase (lattice parameter of ~60 Å) at 8–12% w/w DOG. We suggest that the reduction in lattice parameter and formation of more curved phases upon incorporation of DOPE and DOG is due to the large volume of their alkyl chains compared to the head group region (these molecules have a wedge shape, critical packing parameter or CPP $\gg 1$, whereas the CPP is >1 for MO).[3] This ratio is larger for DOG than for DOPE due to the reduced size of the head group of DOG, consistent with induction of more curved phases in mixtures with MO. We note that DOPE and DOG also form highly curved phases at room temperature and in excess water adopting an inverse hexagonal and fluid isotropic phase respectively (Table 1), consistent with these observations. The increased effect of DOG on the cubic phase architecture relative to DOPE suggests that the dephosphorylation of DOPE to form DOG should result in an overall reduction in lattice parameter of the cubic phase, particularly for systems with a high initial concentration of DOPE.

SAXS results for MO with 0–10% w/w DOPE and 0–18 mg mL^{-1} *Nm*EptA show an increase in lattice parameter with increasing *Nm*EptA concentration for all DOPE concentrations (Fig. 6), providing an indication of a change in the mass fraction of substrate (DOPE) and product (DOG) and progress of the *Nm*EptA enzymatic reaction. The magnitude of this increase was reduced, however, in the presence of DOPE as shown in Fig. 6(A). *i.e.* the presence of a higher concentration of substrate (DOPE) leads to higher *Nm*EptA enzyme activity, leading to a higher concentration

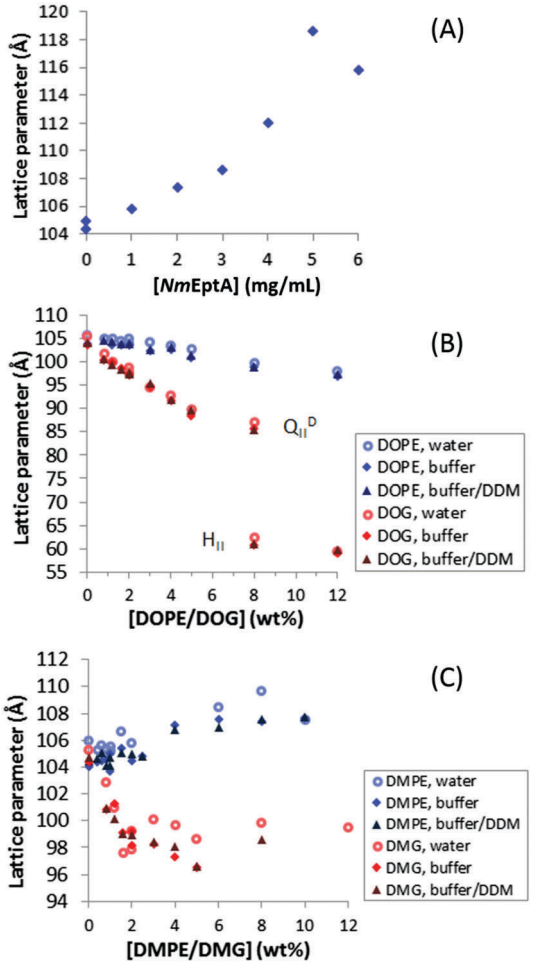

Fig. 5 Lattice parameter in angstrom of the MO diamond cubic Q_{II}^{D} phase (obtained from SAXS analysis) as a function of (A) *Nm*EptA concentration in buffer/DDM as determined after 12 hours using the high-throughput setup. (B) DOPE and DOG concentration in water, buffer and buffer/DDM. In some wells the inverse hexagonal H_{II} phase was observed, as indicated in the graph (lattice parameters ~60 Å). (C) DMPE and DMG concentration in water, buffer and buffer/DDM. (B and C) Were analyzed after 24 hours using the same high-throughput setup.

of product (DOG) and a decrease in the lattice parameter, as DOG reduces MO lattice parameters more significantly than DOPE. This reduction in lattice parameter at higher DOPE concentrations is consistent with *Nm*EptA being active and forming DOG by 12 hours.

A linear fit to the slope of all reproducible data as shown in Fig. 6(A) shows the substrate dependence of the change in lattice parameters and reaction progress and strongly suggests dephosphorylation of DOPE occurred with formation of DOG after 12 hours in the high-throughput assay with samples of ~0.5 μL (Fig. 6(C), all fits of the data in (A) with coefficient of determination or $R^2 > 0.92$), as shown in Fig. 6(C). The effect of forming MOPE on the cubic phase nanostructure is unknown but is expected to be minor. The effect of an additive lipid on phase behavior depends on the concentration of the lipid and its average "shape" as determined by the CPP. The addition of the PEA moiety to the MO lipid should not change the CPP for

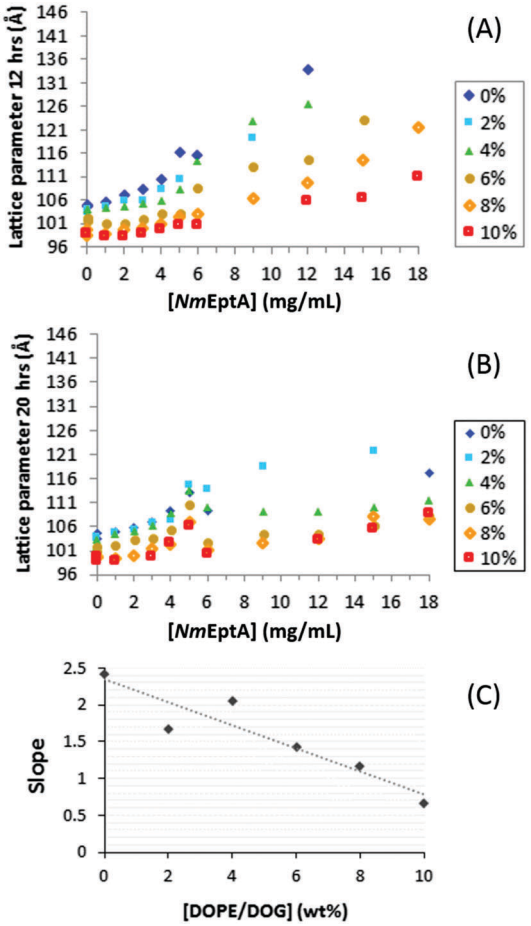

Fig. 6 SAXS results for high-throughput *Nm*EptA assay with DOPE. In (A and B) the lattice parameters in angstrom for the MO diamond cubic Q_{II}^{D} phase (obtained from SAXS analysis) are shown as a function of *Nm*EptA concentration with different concentrations of DOPE (% w/w). Data in (A) are after 12 hours and data in (B) are after 20 hours. In (C) the slope of linear fit results of the data in (A) are shown as a function of DOPE and DOG concentration: fits of the data in (A) all had $R^2 > 0.92$. A linear fit through the data is shown in (C) and this linear decrease is statistically significant: *P*-value = 0.007 (<0.05) as determined using regression analysis in Excel.

this lipid significantly. In addition, as the concentration of MOPE is low (<10% w/w), the effect of this lipid on MO phase behavior is expected to be minor.

Results after 20 hours are shown in Fig. 6(B); the Q_{II}^{D} lattice parameters at high *Nm*EptA concentrations were significantly reduced compared to the results after 12 hours. Small pockets of disorder to accommodate the *Nm*EptA enzyme may have formed within the cubic phase,[47,48] allowing the bulk cubic phase to adapt lattice parameters closer to values without the *Nm*EptA protein. It is also possible that the protein conformation changed within these small samples and after storage at room temperature for one day.

Results obtained under identical conditions after 2 hours were found to be irreproducible, consistent with a previous observation that a time period of several hours is required for full reconstitution of the protein into the cubic phase.[28]

Activity of *Nm*EptA in DMPE doped MO. The activity of *Nm*EptA was also investigated in the presence of the saturated chain phospholipid DMPE, where DMPE causes an increase in Q_{II}^{D} lattice parameters from ~105 Å to ~108 Å at 10% w/w, Fig. 5(C). DMPE at room temperature and in excess water forms the lamellar L_α phase with a lattice parameter of ~51 Å, Table 1. A coexisting L_α phase with similar lattice parameters was observed for cubic phases with a concentration of 6% w/w DMPE and higher, suggesting this molecule has a limited solubility in the MO cubic phase. Flattening of the cubic phase membrane, resulting in an increase in cubic phase lattice parameters, is typical for lipid additives that form the flat lamellar phase in excess water. These lipids tend to have an effectively large head group compared to the chain volume (CPP < 1): the unsaturation in the dioleoyl (DO) chains increases their volume significantly compared to the saturated dimyristoyl (DM) chains. Similar results were found for phospholipids, such as DOPC, in the literature.[39] In contrast, DMG was found to cause a decrease in Q_{II}^{D} lattice parameters from ~105 Å to ~98 Å at 5% w/w. No further effect on Q_{II}^{D} lattice parameters was observed at 5–12% w/w DMG and a coexisting L_α phase with typical lattice parameters for DMG (~42 Å, Table 1) was observed at concentrations of 3% w/w and over. This suggests that at concentrations of 5% w/w and higher no additional DMG was incorporated within the MO cubic phase. Results for DMPE and DMG in the Q_{II}^{D} phase of MO showed that a reduction in cubic phase lattice parameters is expected upon dephosphorylation of DMPE, resulting in the formation of DMG.

SAXS results for MO with 0–10% w/w DMPE and 0–18 mg mL^{-1} *Nm*EptA show an increase in lattice parameter with increasing *Nm*EptA concentration for all DMPE concentrations (Fig. 7), again indicating a change in the mass fraction of substrate (this time DMPE) and product (DOG) and progress of the *Nm*EptA enzymatic reaction. The magnitude of this increase scales with increasing concentration of DMPE, consistent with the formation of the enzymatic product DMG, which reduces the MO lattice parameters (note that DMPE causes an increase). A linear fit through all reproducible data points as shown for each of the DMPE concentrations in Fig. 7(A), with $R^2 > 0.94$, shows a substrate dependence for reaction progress and the lattice parameters and again strongly suggests that DMPE was dephosphorylated forming DMG by 12 hours (Fig. 7(C)). The linear decrease from 0 to 10% w/w DMPE/DMG may not be statistically significant in this case and the reduction in slope was much greater for DOPE, as could be expected. The limited solubility of DMPE and DMG in the cubic phase of MO is consistent with the observation that trends with concentrations of 6% w/w DMPE and higher are less significant (data from 0 to 4% w/w DMPE/DMG do show a statistically significant linear decrease) than with DOPE. This is expected to be due to the limited solubility of the saturated C14 alkyl chains of DMPE and DMG with the singly unsaturated C18 alkyl chains of MO. In contrast, DOPE and DOG have the same alkyl chains as MO, and are therefore expected to be more soluble within the MO bilayer.

Results with DMPE after 20 hours are shown in Fig. 7(B), and the Q_{II}^{D} lattice parameters at high *Nm*EptA concentrations were

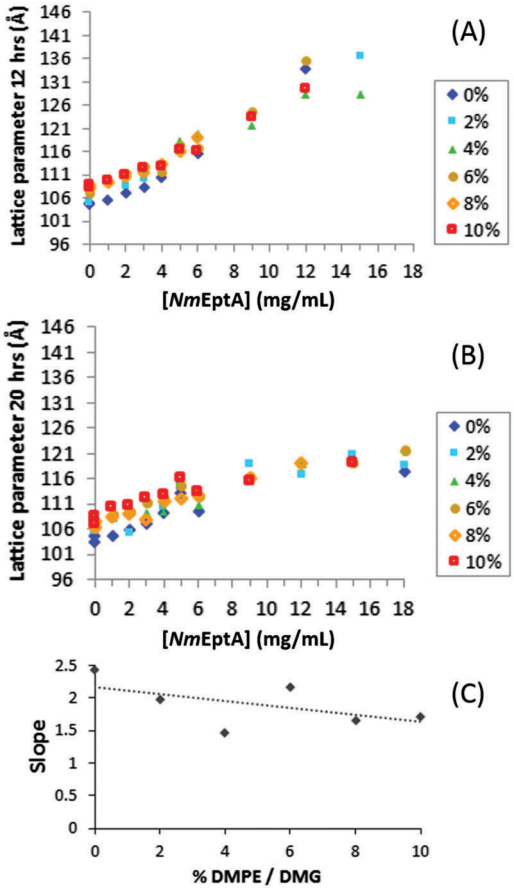

Fig. 7 SAXS results for the high-throughput *Nm*EptA assay with DMPE. In (A and B) the lattice parameters in angstrom for the MO diamond cubic Q_{II}^{D} phase (obtained from SAXS analysis) are shown as a function of *Nm*EptA concentration with different concentrations of DMPE (% w/w). Data in (A) are after 12 hours and data in (B) are after 20 hours. In (C) the slope of linear fit results of data in (A) are shown as a function of DMPE and DMG concentration: fits of the data in (A) all had $R^2 > 0.94$. A linear fit through the data is shown in (C) as a guide for the eye, but the linear decrease is not statistically significant: *P*-value = 0.25 (>0.05) as determined using regression analysis in Excel. This is explained by the limited solubility of DMPE and DMG in the cubic phase of MO at more than 6% w/w; the linear decrease from 0 to 4% w/w DMPE/DMG is statistically significant (*P*-value = 0.02).

again significantly reduced compared to the results after 12 hours, consistent with the results with DOPE. The results after 2 hours were again irreproducible confirming a time frame of more than 2 hours was needed for the samples to equilibrate.

The high-throughput *Nm*EptA assay results confirmed conversion of a significant amount of the DOPE and DMPE to DOG and DMG respectively after 12 hours in samples that were ~100 times smaller than in the initial bulk phase *Nm*EptA assay. Enzyme conversion rates might differ depending on the sample size. At the lowest *Nm*EptA concentrations studied enzyme activity could already be detected. At the highest *Nm*EptA concentration used in this study, 18 mg mL^{-1}, no saturation of enzyme activity was observed. This shows that high-throughput methods can be used to screen a wide range of *Nm*EptA enzyme concentrations. For DOPE and DMPE we can observe the dephosphorylation at all PEA concentrations, even though at low concentrations the diffusion of the protein and the substrate within the lipid bilayer is slow. Detection of enzyme activity in 96-well plates using SAXS reinforces the prospective nature of high-throughput sample preparation and analysis as a screening tool for drug discovery and in biosensors.

Conclusions

In this study, the enzyme activity of the large amphiphilic *Nm*EptA enzyme upon encapsulation in the nanostructured bicontinuous cubic phase was studied using ESI-TOF MS and HPLC analysis, as well as high-throughput techniques including SAXS analysis. We showed that the *Nm*EptA enzyme was active when encapsulated in the cubic phase. Transfer of the PEA group from DOPE or DMPE to MO, the cubic phase forming lipid, was shown. These data demonstrate that the reaction of *Nm*EptA is not specific to the alkyl chain identity of the donor or receiver substrate. *In vivo* the donor substrate is typically a phospholipid, such as DMPE, and the receiver substrate the lipid A containing lipo-oligosaccharide. SAXS analysis additionally showed that *Nm*EptA caused a swelling of the diamond cubic Q_{II}^{D} phase, shown by a ~25% increase in lattice parameter, due to the presence of the large hydrophilic domain in the nanoscale water channels. At the lowest *Nm*EptA concentrations used, enzyme activity could be detected. At the highest *Nm*EptA concentrations used in this study enzyme activity was still observed, potentially due to the relatively large surface area to volume ratio of the nanostructured bicontinuous cubic phase. This shows that high-throughput methods can be used for both high and low *Nm*EptA concentrations, reinforcing the prospect of using high-throughput sample preparation and analysis as a drug screening tool and in biosensors. The observed rate of enzyme activity was comparable to other membrane bound enzymes, with complete transfer of the PEA group occurring *in vitro*, under the conditions studied, over a 24 hour timescale. This is surprising considering the large hydrophilic domain must be confined within the nanoscale water channels of the cubic phase, and disordered nanopockets to accommodate the *Nm*EptA enzyme might have formed.

Acknowledgements

We thank Drs Adrian M. Hawley, Stephen T. Mudie, Nigel M. Kirby and Timothy M. Ryan for their assistance with SAXS experiments, and we acknowledge use of the SAXS/WAXS beamline at the Australian Synchrotron. We thank Dr Janet Newman for help with the robotic setup of plates at the C^3 Collaborative Crystallization Centre, CSIRO, Parkville, Australia. We acknowledge Dr Ching-Seng Ang for help with RP-HPLC and ESI-TOF MS measurements. Ms Leonie van 't Hag is supported by a Melbourne International Research Scholarship and a CSIRO PhD scholarship. Ms Anandhi Anandan acknowledges support through a Fay Gale Fellowship from the University of Western Australia. A/Prof. Sally L. Gras is supported by the ARC Dairy Innovation Hub IH120100005. Funding support to Prof. Alice Vrielink from the National Health

and Medical Research Council of Australia is acknowledged (APP1003697 and APP1078642). Dr Charlotte Conn is the recipient of an ARC DECRA Fellowship DE160101281.

References

1 C. E. Conn and C. J. Drummond, *Soft Matter*, 2013, **9**, 3449–3464.
2 V. Luzzati, A. Tardieu, T. Gulikkrz, E. Rivas and F. Reisshus, *Nature*, 1968, **220**, 485–488.
3 C. Fong, T. Le and C. J. Drummond, *Chem. Soc. Rev.*, 2012, **41**, 1297–1322.
4 E. M. Landau and J. P. Rosenbusch, *Proc. Natl. Acad. Sci. U. S. A.*, 1996, **93**, 14532–14535.
5 X. Mulet, B. J. Boyd and C. J. Drummond, *J. Colloid Interface Sci.*, 2013, **393**, 1–20.
6 A. Zabara and R. Mezzenga, *J. Controlled Release*, 2014, **188**, 31–43.
7 A. Angelova, B. Angelov, V. M. Garamus, P. Couvreur and S. Lesieur, *J. Phys. Chem. Lett.*, 2012, **3**, 445–457.
8 S. M. Sagnella, X. Gong, M. J. Moghaddam, C. E. Conn, K. Kimpton, L. J. Waddington, I. Krodkiewska and C. J. Drummond, *Nanoscale*, 2011, **3**, 919–924.
9 J. Zhai, J. A. Scoble, N. Li, G. Lovrecz, L. J. Waddington, N. Tran, B. W. Muir, G. Coia, N. Kirby, C. J. Drummond and X. Mulet, *Nanoscale*, 2015, **7**, 2905–2913.
10 J. J. Vallooran, S. Handschin, S. M. Pillai, B. N. Vetter, S. Rusch, H.-P. Beck and R. Mezzenga, *Adv. Funct. Mater.*, 2016, **26**, 181–190.
11 E. Nazaruk, S. Smolinski, M. Swatko-Ossor, G. Ginalska, J. Fiedurek, J. Rogalski and R. Bilewicz, *J. Power Sources*, 2008, **183**, 533–538.
12 Y. L. Liang, C. E. Conn, C. J. Drummond and C. Darmanin, *J. Colloid Interface Sci.*, 2015, **441**, 78–84.
13 L. van't Hag, X. Li, T. G. Meikle, S. V. Hoffmann, N. C. Jones, J. S. Pedersen, A. M. Hawley, S. L. Gras, C. E. Conn and C. J. Drummond, *Langmuir*, 2016, **32**, 6882–6894.
14 L. van't Hag, H.-H. Shen, T.-W. Lin, S. L. Gras, C. J. Drummond and C. E. Conn, *Langmuir*, 2016, **32**, 12442–12452.
15 L. van't Hag, H. H. Shen, J. X. Lu, A. M. Hawley, S. L. Gras, C. J. Drummond and C. E. Conn, *Langmuir*, 2015, **31**, 12025–12034.
16 A. Zabara, R. Negrini, O. Onaca-Fischer and R. Mezzenga, *Small*, 2013, **9**, 3602–3609.
17 B. Angelov, A. Angelova, S. K. Filippov, M. Drechsler, P. Stepanek and S. Lesieur, *ACS Nano*, 2014, **8**, 5216–5226.
18 M. Caffrey and V. Cherezov, *Nat. Protoc.*, 2009, **4**, 706–731.
19 A. Misiunas, Z. Talaikyte, G. Niaura, V. Razumas and T. Nylander, *Biophys. Chem.*, 2008, **134**, 144–156.
20 T. Nylander, C. Mattisson, V. Razumas, Y. Miezis and B. Hakansson, *Colloids Surf., A*, 1996, **114**, 311–320.
21 V. Razumas, J. Kanapieniene, T. Nylander, S. Engstrom and K. Larsson, *Anal. Chim. Acta*, 1994, **289**, 155–162.
22 W. Sun, J. J. Vallooran, A. Zabara and R. Mezzenga, *Nanoscale*, 2014, **6**, 6853–6859.
23 W. J. Sun, J. J. Vallooran and R. Mezzenga, *Langmuir*, 2015, **31**, 4558–4565.
24 E. Nazaruk, R. Bilewicz, G. Lindblom and B. Lindholm-Sethson, *Anal. Bioanal. Chem.*, 2008, **391**, 1569–1578.
25 W. J. Sun, J. J. Vallooran, W. K. Fong and R. Mezzenga, *J. Phys. Chem. Lett.*, 2016, **7**, 1507–1512.
26 C. Speziale, L. Salvati Manni, C. Manatschal, E. M. Landau and R. Mezzenga, *Proc. Natl. Acad. Sci. U. S. A.*, 2016, **113**, 7491–7496.
27 N. H. Joh, T. Wang, M. P. Bhate, R. Acharya, Y. B. Wu, M. Grabe, M. Hong, G. Grigoryan and W. F. DeGrado, *Science*, 2014, **346**, 1520–1524.
28 C. Darmanin, S. Sarkar, L. Castelli and C. E. Conn, *Cryst. Growth Des.*, 2016, **16**, 5014–5022.
29 C. G. Tate and G. F. X. Schertler, *Curr. Opin. Struct. Biol.*, 2009, **19**, 386–395.
30 A. Wise, K. Gearing and S. Rees, *Drug Discovery Today*, 2002, **7**, 235–246.
31 C. V. Kulkarni, W. Wachter, G. Iglesias-Salto, S. Engelskirchen and S. Ahualli, *Phys. Chem. Chem. Phys.*, 2011, **13**, 3004–3021.
32 J. Briggs, H. Chung and M. Caffrey, *J. Phys. II*, 1996, **6**, 723–751.
33 H. Qiu and M. Caffrey, *Biomaterials*, 2000, **21**, 223–234.
34 T. G. Meikle, C. E. Conn, F. Separovic and C. J. Drummond, *RSC Adv.*, 2016, **6**, 68685–68694.
35 L. van't Hag, L. de Campo, C. J. Garvey, G. C. Feast, A. E. Leung, N. R. Yepuri, R. Knott, T. L. Greaves, N. Tran, S. L. Gras, C. J. Drummond and C. E. Conn, *J. Phys. Chem. Lett.*, 2016, **7**, 2862–2866.
36 C. Wanty, A. Anandan, S. Piek, J. Walshe, J. Ganguly, R. W. Carlson, K. A. Stubbs, C. M. Kahler and A. Vrielink, *J. Mol. Biol.*, 2013, **425**, 3389–3402.
37 P. Sperandeo, G. Deho and A. Polissi, *Biochim. Biophys. Acta, Mol. Cell Biol. Lipids*, 2009, **1791**, 594–602.
38 C. M. John, M. F. Liu, N. J. Phillips, Z. J. Yang, C. R. Funk, L. I. Zimmerman, J. M. Griffiss, D. C. Stein and G. A. Jarvis, *Infect. Immun.*, 2012, **80**, 4014–4026.
39 V. Cherezov, J. Clogston, Y. Misquitta, W. Abdel-Gawad and M. Caffrey, *Biophys. J.*, 2002, **83**, 3393–3407.
40 C. Darmanin, C. E. Conn, J. Newman, X. Mulet, S. A. Seabrook, Y. L. Liang, A. Hawley, N. Kirby, J. N. Varghese and C. J. Drummond, *ACS Comb. Sci.*, 2012, **14**, 247–252.
41 N. M. Kirby, S. T. Mudie, A. M. Hawley, D. J. Cookson, H. D. T. Mertens, N. Cowieson and V. Samardzic-Boban, *J. Appl. Crystallogr.*, 2013, **46**, 1670–1680.
42 J. M. Seddon, A. M. Squires, C. E. Conn, O. Ces, A. J. Heron, X. Mulet, G. C. Shearman and R. H. Templer, *Philos. Trans. R. Soc., A*, 2006, **364**, 2635–2655.
43 L. van't Hag, C. Darmanin, T. C. Le, S. Mudie, C. E. Conn and C. J. Drummond, *Cryst. Growth Des.*, 2014, **14**, 1771–1781.
44 N. B. Cech and C. G. Enke, *Mass Spectrom. Rev.*, 2001, **20**, 362–387.
45 P. Juaneda and G. Rocquelin, *Lipids*, 1986, **21**, 239–240.

46 S. J. Ullrich, U. A. Hellmich, S. Ullrich and C. Glaubitz, *Nat. Chem. Biol.*, 2011, **7**, 263–270.
47 A. Angelova, B. Angelov, R. Mutafchieva, S. Lesieur and P. Couvreur, *Acc. Chem. Res.*, 2011, **44**, 147–156.
48 A. Angelova, M. Ollivon, A. Campitelli and C. Bourgaux, *Langmuir*, 2003, **19**, 6928–6935.
49 P. O. Eriksson and G. Lindblom, *Biophys. J.*, 1993, **64**, 129–136.
50 D. F. Parsons, M. Bostrom, P. Lo Nostro and B. W. Ninham, *Phys. Chem. Chem. Phys.*, 2011, **13**, 12352–12367.
51 X. Ai and M. Caffrey, *Biophys. J.*, 2000, **79**, 394–405.
52 C. E. Conn, C. Darmanin, S. M. Sagnella, X. Mulet, T. L. Greaves, J. N. Varghese and C. J. Drummond, *Soft Matter*, 2010, **6**, 4828–4837.
53 R. H. Templer, K. H. Madan, N. A. Warrender and J. M. Seddon, in *The Structure and Conformation of Amphiphilic Membranes: Proceedings of the International Workshop on Amphiphilic Membranes, Jülich, Germany, September 16–18, 1991*, ed. R. Lipowsky, D. Richter and K. Kremer, Springer Berlin Heidelberg, Berlin, Heidelberg, 1992, pp. 262–265, DOI: 10.1007/978-3-642-84763-9_51.